On the Wavelength of the Rossby Waves Radiated by Tropical Cyclones

KYLE D. KROUSE

Department of Applied Physics and Applied Mathematics, Columbia University, New York, New York

ADAM H. SOBEL AND LORENZO M. POLVANI

Department of Applied Physics and Applied Mathematics, and Department of Earth and Environmental Sciences, Columbia University, New York, New York

(Manuscript received 11 January 2007, in final form 16 April 2007)

ABSTRACT

The authors present a theory for the zonal wavelength of tropical depression–type disturbances, which occur as a result of Rossby wave radiation from a preexisting tropical cyclone (TC). In some cases, such disturbances undergo tropical cyclogenesis, resulting in a pair of tropical cyclones; the theory then predicts the zonal separation distance of such tropical cyclone pairs.

Numerical experiments are presented in which a thermally forced vortex, superimposed on an initial state of rest, is moved at different velocities in a shallow-water model on a sphere. Vortices moving westward generate coherent wave trains to the east or southeast (depending on the amplitude of the vortex), resembling those in observations. The zonal wavelengths of these wave trains in each case are well described by the linear stationary solution in the frame comoving with the vortex. Vortices moving eastward or remaining stationary do not generate such trains, also consistent with linear theory, which admits no stationary solutions in such cases. It is hypothesized that the wavelengths of observed disturbances are set by the properties of the relevant stationary solution. The environmental flow velocity that determines this wavelength is not the translation velocity of the tropical cyclone, but the difference between the steering flow of the radiated Rossby waves and that of the TC. The authors argue that either horizontal or vertical shear in the environment of the TC can generate differences between these steering flows of the necessary magnitude and sign to generate the observed wavelengths.

1. Introduction

A tropical cyclone (TC) is a strong, thermally forced vortex. In the presence of a large-scale potential vorticity gradient, such a vortex will radiate Rossby waves (e.g., McWilliams and Flierl 1979; Flierl et al. 1983; McWilliams et al. 1986; Shapiro and Ooyama 1990; Ferreira and Schubert 1997). In the tropical cyclone literature, this process is sometimes referred to as "eastward energy dispersion." It results in the development of an anticyclonic disturbance to the east of the TC and a cyclonic one to the east of that, typically 2000–3000 km from the TC. This second cyclonic disturbance is sometimes the site of new tropical cyclogenesis (Frank 1982; Davidson and Hendon 1989; Carr and Elsberry 1995; Holland 1995; Briegel and Frank 1997; Ritchie and Holland 1999; Li et al. 2003; Li and Fu 2006). We refer to such events as "multiple cyclone events."

In other cases, the second disturbance may not undergo genesis but remain as a weaker disturbance, of the sort sometimes known as "easterly waves" or "tropical depression–type" (TD-type) disturbances (Reed and Recker 1971; Nitta and Takayabu 1985; Lau and Lau 1990; Takayabu and Nitta 1993; Dunkerton and Baldwin 1995; Chang et al. 1996). While these disturbances have been extensively studied, basic questions remain about their dynamics. The fundamental mechanism by which they are generated is not known and, relatedly, no theory exists for their spatial and temporal scales. Some recent studies have argued that "wave accumulation" (Webster and Chang 1988; Chang and Webster 1990, 1995) may be involved in the development of these disturbances (Holland 1995; Sobel and Bretherton 1999; Sobel and Maloney 2000; Kuo et al.

Corresponding author address: Kyle D. Krouse, 500 W. 120th Street, Room 200, Columbia University, New York, NY 10027.
E-mail: kdk8@columbia.edu

DOI: 10.1175/2007JAS2402.1

2001; Dickinson and Molinari 2002; Aiyyer and Molinari 2003). Even if correct, this argument does not imply any particular spatial scale, only that the disturbance intensifies as the spatial scale reduces.

Sobel and Bretherton (1999) argued that since TCs occur frequently in the western North Pacific, Rossby wave radiation from TCs might be a climatologically important mechanism for the generation of TD-type disturbances. In this study, we examine this radiation process more closely, using numerical solutions of the shallow-water equations and elementary analytical considerations. We use a simple linear argument to explain the wavelengths of disturbances radiated from a forced vortex. If correct, this argument explains the spatial scale of some TD-type disturbances in the western North Pacific and also the separation distance of pairs of tropical cyclones in multiple cyclone events that form due to the eastward energy dispersion mechanism.

The paper is laid out as follows: In section 2 we describe the numerical model, the simulation design, and the methods used to analyze the results. In section 3 we offer the key results: those at low forcing amplitude are presented in section 3a, followed by an interpretation section 3b, where the essence of our theory, as it is hypothesized to be relevant to the observations, is spelled out. In section 3c we discuss the role of nonlinearity, as it appears in simulations using a larger amplitude than those in section 3a. In section 4 we give a brief summary and some conclusions.

2. Methods

We employ a nonlinear shallow-water model on the sphere. A localized mass sink, formulated as a Newtonian relaxation of the height field toward a specified function of position and time, which has an isolated minimum, is used to generate a strong localized vortex, which is our simple representation of a tropical cyclone. This sink is moved with a constant velocity in the zonal direction with a speed $-U$. The minus sign is used so that U represents the environmental flow speed in the frame of reference moving with the mass sink, as explained further in sections 3a and 3b.

The model equations are those of the shallow-water system in spherical coordinates:

$$\frac{\partial u}{\partial t} + \mathbf{u}\cdot\boldsymbol{\nabla} u - \left(f + \frac{u}{a}\tan\theta\right)v = -\frac{g}{a\cos\theta}\frac{\partial h}{\partial \lambda} + \mu_4\nabla^4 u, \tag{1a}$$

$$\frac{\partial v}{\partial t} + \mathbf{u}\cdot\boldsymbol{\nabla} v + \left(f + \frac{u}{a}\tan\theta\right)u = -\frac{g}{a}\frac{\partial h}{\partial \theta} + \mu_4\nabla^4 v, \tag{1b}$$

$$\frac{\partial h}{\partial t} + \mathbf{u}\cdot\boldsymbol{\nabla} h + \frac{h}{a\cos\theta}\left(\frac{\partial u}{\partial \lambda} + \frac{\partial v\cos\theta}{\partial \theta}\right) = \frac{h_f - h}{\tau} + \mu_4\nabla^4 h. \tag{1c}$$

The notation is standard: $\mathbf{u} = (u, v)$ is the horizontal wind, (θ, λ) are latitude and longitude respectively, g is the gravitational acceleration constant, a is the mean radius of the earth, f is the local value of the Coriolis parameter, and h is the fluid depth. The standard hyperdiffusion, with a ∇^4 operator, is employed in our computations to inhibit the cascade of enstrophy to the smallest resolvable scales. The coefficient μ_4 is varied with the resolution and is chosen so that the smallest scales resolved by the model are damped with a time scale of approximately ⅔ day.

The first term on the rhs of Eq. (1c) is the thermal forcing, used to induce a TC-like vortex. The size, shape, and amplitude of the vortex are imposed by the choice of the function h_f, as well as the time scale τ; no attempt is made to explicitly model the moist convection that drives TCs in nature. The thermal forcing function $h_f(\theta, \lambda, t)$ has the form

$$h_f(\theta, \lambda, t) = H_0 + (H_{\min} - H_0) \times \exp\left(-\left\{\frac{\xi[\theta, \lambda; \theta_0(t), \lambda_0(t)]}{\xi_0}\right\}^2\right). \tag{2}$$

The constant term, H_0, is chosen to be 250 m. This value corresponds to a gravity wave speed of approximately 50 m s^{-1}, appropriate for dry gravity waves with a first baroclinic mode structure (e.g., Fulton and Schubert 1985; Mapes and Houze 1995). Spectral analysis of outgoing longwave radiation anomalies by Wheeler and Kiladis (1999) suggests somewhat smaller equivalent depths for moist "convectively coupled" waves. We have performed simulations using depths as small as 25 m. While the wavelength of the response varies slightly with the choice of H_0 (as, to be shown, expected from the dispersion relation for Rossby waves), the results of these simulations are very similar to those using 250 m, so we present only the latter.

The amplitude $H_{\min}$ of the mass sink is varied to sample a range of amplitudes, covering regimes that are primarily characterized by linear dynamics as well as more nonlinear regimes. The degree of nonlinearity is measured by the Rossby number, defined as the spatial and temporal maximum of relative vorticity divided by the value of the planetary vorticity at that point: $\mathrm{Ro} = \zeta_{\max}(\theta, \lambda, t)/f(\theta)$. For the "linear" experiments presented in section 3a we use $H_{\min} = 150$ m and for the

"nonlinear" ones in section 3c we use $H_{\min} = -250$ m. The system responds in such a way that even in the nonlinear cases the actual fluid depth never becomes zero or negative. The minimum in h_f is located at $[\theta_0(t), \lambda_0(t)]$, the latitude and longitude of the imposed trajectory. In all of the results presented (save Fig. 6) the latitude remains constant at 15°N. The vortex is moved zonally at a speed $-U$ so that $[\theta_0(t), \lambda_0(t)] = (15°\text{N}, -Ut)$.

Experiments were also performed by varying the latitude of the minimum of the forcing θ_0 in 5° increments from the equator to 40°N. The results of these experiments are qualitatively very similar to one another, but with the response shifted latitudinally with the forcing.

The expression $\xi[\theta, \lambda; \theta_0(t), \lambda_0(t)]$ is the angle on the sphere between the point on the sphere (θ, λ) and the location of the minimum of the mass sink $[\theta_0(t), \lambda_0(t)]$.[1] The denominator, ξ_0, is a measure of the width of the vortex. Setting $\xi_0 \cong 8.5°$ for the experiments run at T42 spectral resolution and $\xi_0 \cong 5.0°$ for those run at T85 resolution results in vortices of approximately 3000 and 1800 km in width, respectively, about as small as can be comfortably resolved in each case.

We also vary the value of the relaxation time scale $\tau(\theta, \lambda, t)$ in space and in time, giving it a Gaussian form with the same scale as that used for h_f:

$$\tau(\theta, \lambda, t) = \tau_0 + (\tau_{\min} - \tau_0) \times \exp\left(-\left\{ \frac{\xi[\theta, \lambda; \theta_0(t), \lambda_0(t)]}{\xi_0} \right\}^2 \right), \quad (3)$$

where $\tau_{\min}$ is the minimum time scale, occurring near the vortex center and τ_0 is the far-field time scale. The angles $\xi[\theta, \lambda; \theta_0(t), \lambda_0(t)]$ and ξ_0 are the same as described above. In all of our simulations, $\tau_{\min} = 36$ h and $\tau_0 = 10$ days. The small value near the vortex center is chosen so as to drive the vortex strongly. In the far field, the dynamical role of the thermal forcing term is primarily that of a damping on the waves radiated from the vortex. A long time scale in this region corresponds to a weak damping on those waves.

We use the spherical transform shallow-water model (STSWM) to solve Eqs. (1a)–(1c). STSWM was developed at the National Center for Atmospheric Research (NCAR) and solves the shallow-water equations on the sphere using a pseudospectral spatial discretization and a semi-implicit leapfrog time stepping (Hack and Jakob 1992). The results presented in this paper were obtained at T42 and T85 spectral resolutions with $\mu_4 = 1.0 \times 10^{16}$ m^4 s^{-1} for the T42 runs and $\mu_4 = 6.25 \times 10^{14}$ m^4 s^{-1} for the T85 runs.

[1] The exact expression for the angle between two points on the sphere, $\xi(\theta, \lambda; \theta_0, \lambda_0)$, is given by $\xi(\theta, \lambda; \theta_0, \lambda_0) = \arccos[\cos(\theta_0)\cos(\lambda_0)\cos(\theta)\cos(\lambda) + \cos(\theta_0)\sin(\lambda_0)\cos(\theta)\sin(\lambda) + \sin(\theta_0)\sin(\theta)]$.

3. Results

a. Linear regime, Ro < 1

Figure 1, at spectral resolution T85, shows the relative vorticity field for three values of U. The values are -5, 0, and $+5$ m s^{-1}, corresponding to imposed eastward motion, no motion, or westward motion of the mass sink. Recall that U does not represent the zonal translation velocity of the TC but rather its opposite, the environmental flow in the frame comoving with the TC. This makes comparison with standard linear wave theory more straightforward.

Our computations are performed over the whole sphere; only the relevant portion of the results is presented here. From an initially quiescent state with a uniform depth $h = H_0$, we spin up the vortices using the Gaussian mass sink and forcing time scale described in Eqs. (2) and (3). Snapshots of ζ are shown starting at day 2, the time when the vortex has fully spun up, and at 3-day intervals thereafter. The average value of Ro over the three runs is 0.46. Only in the last column, $U = +5$ m s^{-1} (corresponding to westward motion of the mass sink), does a wave train form. This structure is stationary in a frame moving with the mass sink.

The first two columns show the development of zonally elongated "beta plumes" but no structures that could be called wavelike in the zonal direction. This behavior is familiar from previous work using a stationary mass source in the presence of the β effect (e.g., Hsu and Plumb 2000).

The development of a stationary wave train in the case of a westward-moving vortex, but not a stationary or eastward-moving one, can be easily understood within the framework of standard linear Rossby wave dynamics. Consider the well-known shallow-water dispersion relation that results from linearizing the shallow-water equations about a state of rest, making the equatorial β-plane approximation ($f = \beta_0 y$).

Following Matsuno (1966) and Gill (1982, chapter 11),

$$\frac{\omega^2}{c^2} - \frac{\beta_0 k}{\omega} - k^2 = \frac{2n+1}{R_{\text{eq}}^2}, \quad (4)$$

where $c = \sqrt{gH_0}$, H_0 is the mean depth of the system, β_0 is the meridional gradient of planetary vorticity, k is

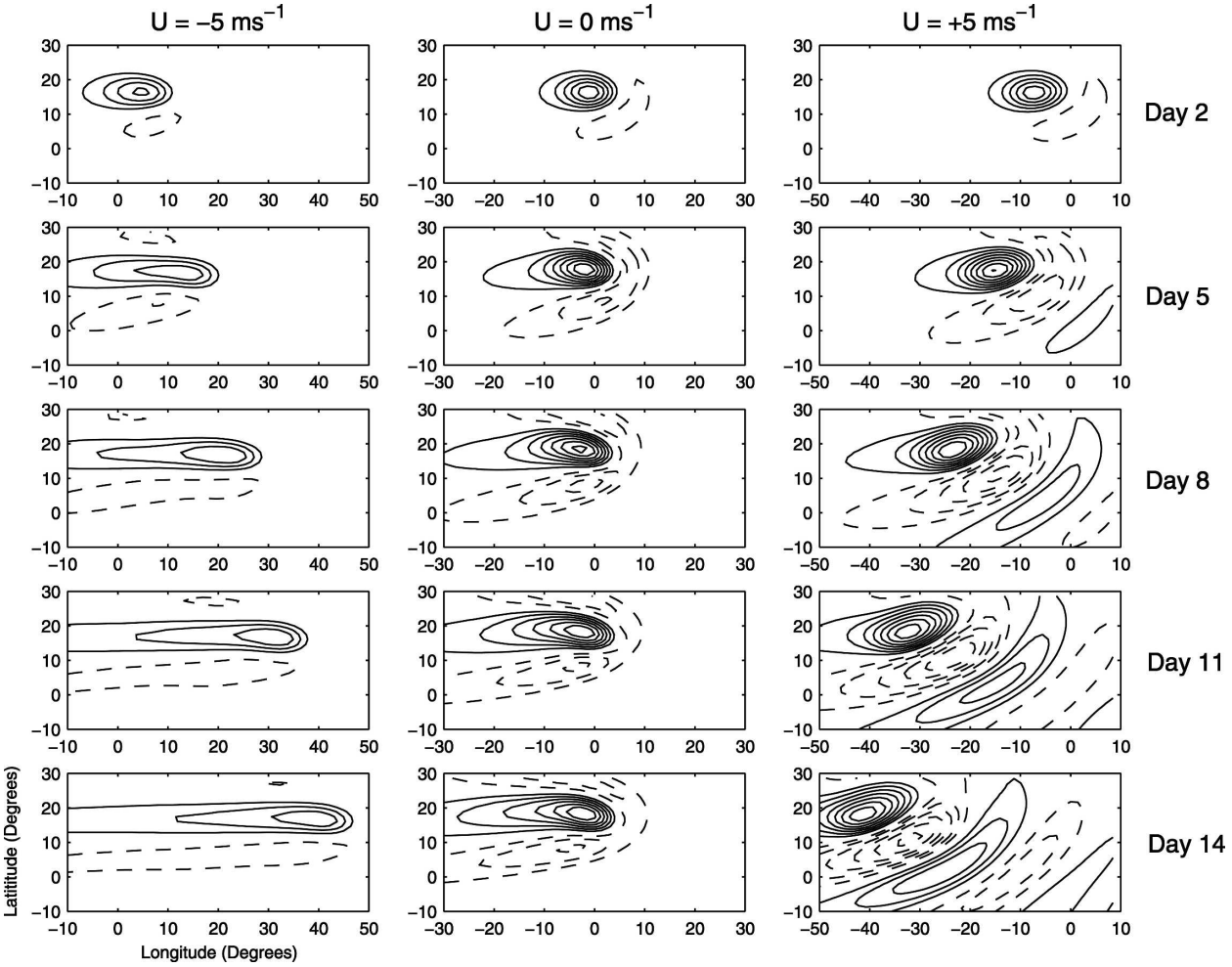

FIG. 1. Time evolution of the relative vorticity ζ, at 3-day intervals: contour interval 0.25×10^{-5} m s^{-1}. Columns correspond to $U = -5$, 0, and $+5$ m s^{-1}. The average Rossby number in this linear regime is Ro = 0.46. Note that the Rossby wave train only develops for $U = +5$ m s^{-1} with the dominant wavelength in the wake becoming time-independent while amplitudes grow in time, indicating eastward energy dispersion from short Rossby waves.

the zonal wavenumber, n is the meridional integer wavenumber, and $R_{eq} = \sqrt{c/\beta_0}$ is the equatorial Rossby radius of deformation.

At low frequencies (small ω), Eq. (4) becomes approximately

$$\omega = \frac{-\beta_0 k}{k^2 + (2n+1)R_{eq}^{-2}}. \tag{5}$$

Equation (5) admits no stationary solutions for $k \neq 0$. If we add a uniform background zonal flow with velocity U, the dispersion relation becomes

$$\omega = \frac{-\beta_0 k}{k^2 + (2n+1)R_{eq}^{-2}} + kU, \tag{6}$$

which has a stationary solution at a nonzero k,

$$k = \sqrt{\frac{\beta_0}{U} - (2n+1)R_{eq}^{-2}}, \tag{7}$$

which is real provided $\beta_0/U > (2n+1)R_{eq}^{-2}$. For U positive but not too large, this can be satisfied for sufficiently small values of n. For U negative or zero, it cannot be satisfied.

This is illustrated in Fig. 2, where we have plotted the curves for ω versus k from the dispersion relation (6) for the three values $U = -5$, 0, and $+5$ m s^{-1}, in all cases for the $n = 1$ meridional mode. Note that only in the case $U > 0$ does a stationary solution exist (corresponding to a real value of k), indicated by the small

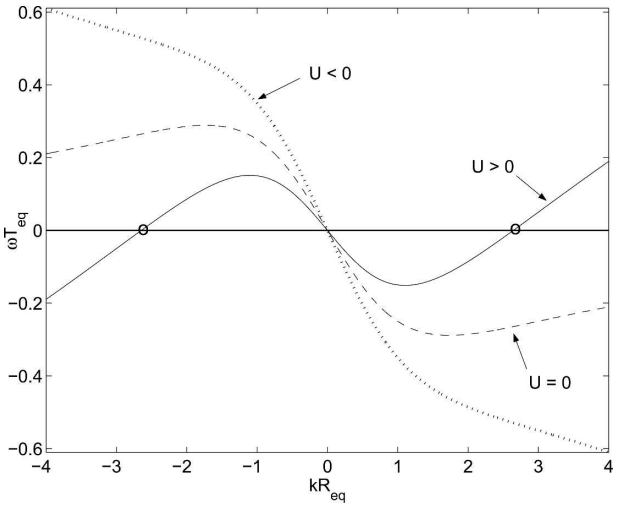

FIG. 2. The $n = 1$ meridional mode's dispersion relation [Eq. (6)] for $U = -5$ m s^{-1} (dotted), $U = 0$ m s^{-1} (dashed), and for $U = +5$ m s^{-1} (solid). The axes are nondimensional. The stationary solution (circled) corresponds to a wavelength (for $U = 5$ m s^{-1}) $\lambda \cong 3000$ km. There are no meaningful stationary solutions for $U \leq 0$.

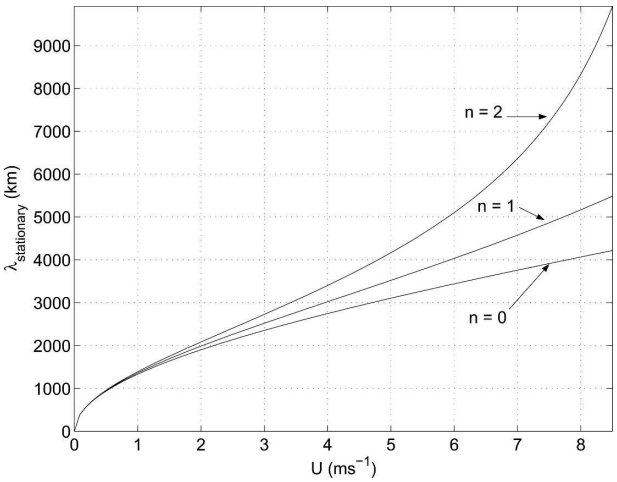

FIG. 3. Wavelengths of stationary solutions vs U [Eq. (8)] for $n = 0, 1, 2$ and $c = 50$ m s^{-1}.

circles. A qualitatively similar pattern occurs for all other meridional modes.

If we look for a solution stationary in the frame moving with our imposed mass sink, U must be interpreted as the background flow in that frame, which is equal and opposite to the translation velocity of the mass sink itself, since the basic state in our simulations is one of rest in the frame stationary with respect to the planet's surface. Our choice of the minus sign on the velocity U in our description of our numerical experiments (see section 2) makes U the appropriate velocity for using Eqs. (6) and (7) to interpret our results. The existence of a stationary solution in our experiments for $U > 0$ but not $U \leq 0$ demonstrates qualitative consistency between our simulations and linear theory; we show below that there is quantitative agreement as well.

The wavelength of the stationary solution, $\lambda = 2\pi/k$, can be written as

$$\lambda_{\text{stationary}} = 2\pi R_{\text{eq}} \sqrt{\frac{1}{c/U - (2n+1)}}. \tag{8}$$

Taking $c = 50$ m s^{-1}, we plot Eq. (8) in Fig. 3 for $n = 0, 1, 2$. We show next that the wavelengths obtained in our simulations are approximately consistent with Eq. (8).

The zonal wavelength of the stationary solution depends upon c, which is set by our choice of the mean depth of the shallow water system, U, which we control by imposing a zonal velocity on the mass sink and n, the meridional wavenumber. To separate the response (specifically, the ζ field) into its different meridional components, a spectral decomposition is performed using the parabolic cylinder functions $D_n(y)$, where y is distance from the equator. To be more precise, one ought to use Hough functions, which are the eigenfunctions of the linearized, unforced, spherical shallow-water equations (the Laplace tidal equations). However, these are cumbersome to compute. For equatorially trapped disturbances, the use of the parabolic cylinder functions, which are the eigenfunctions of the equatorial β-plane problem, yields sufficiently accurate decompositions.

The parabolic cylinder functions are

$$D_n(y) = \exp\left(-\frac{y^2}{2R_{\text{eq}}^2}\right) H_n\left(\frac{y}{R_{\text{eq}}}\right), \tag{9}$$

where (x, y) are the Cartesian longitudinal and latitudinal distances, respectively, and $H_n(z)$ is the nth-order Hermite polynomial.

After projecting the vorticity field onto the $D_n(y)$ eigenfunctions, we are left with a function of longitudinal distance, $f(x)$, for each n:

$$f(x) = \frac{\int_{\text{SP}}^{\text{NP}} D_n(y)\zeta(x, y)\, dy}{\int_{\text{SP}}^{\text{NP}} D_n(y) D_n(y)\, dy}, \tag{10}$$

where (θ, λ) are the latitude and longitude (in radians), respectively, and $x = a\lambda \cos\theta$ and $y = a\theta$. For the positive U experiments, the functions $f(x)$ have the character of wave packets, at least for small n; an example is shown in Fig. 4. We wish to determine a dominant

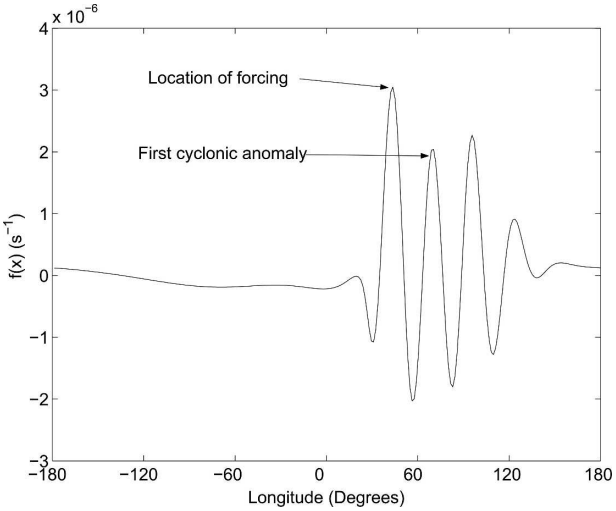

FIG. 4. A typical example of the zonal function $f(x)$ that results from projection onto the $n = 1$ meridional mode. Such projections typically reach equilibrium within a few days.

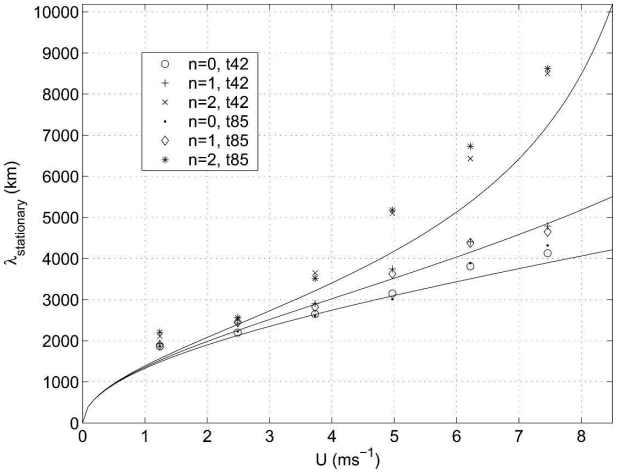

FIG. 5. Solid lines: stationary wavelengths from linear theory, as computed from Eq. (8), as a function of U. Symbols: wavelength extracted from the time integrations, as described in the text, for different meridional wavenumbers and for experiments at various resolutions.

wavelength, which can be compared to the analytical result, Eq. (8).

We do this by measuring the peak-to-peak distance from the forced vortex to the first cyclonic anomaly induced in its wake. After the zonal function $f(x)$ has reached steady state (which usually occurs after about two days), we first apply a cubic spline interpolation to the data and then determine the location of the peaks. We measure this peak-to-peak distance to extract a dominant wavelength because in observations often only a single wavelength—a TC and a second disturbance to its east or southeast—is evident. An alternate approach, using the Fourier spectrum of $f(x)$ to extract a dominant wavelength, has also been used and gives similar results (not shown).

In Fig. 5 we give a direct comparison of the dominant zonal wavelength extracted from the numerical solutions (for $n = 0, 1, 2$) to the separation distance predicted by Eq. (8) from the simple linear arguments above. Results from six different values of U in the interval $0 < U < 8$ m s^{-1} are plotted for both T42 and T85 resolutions. The agreement is quite good, particularly for the smallest values of n. As mentioned in section 2, the results are qualitatively similar over a wide range of values for c. This similarity is presumably due to the fact that, even in the experiments with the smallest mean depth H_0, the relevant gravity wave frequencies are still much larger than those of the Rossby waves, so we are still seeing essentially balanced dynamics.

As also mentioned in section 2, the results are qualitatively independent (up to a latitudinal shift) of the forcing latitude θ_0 as well. In the top panel of Fig. 6, the relative vorticity field that results from a typical linear run (Ro = 0.52) with a low-latitude forcing ($\theta_0 = 7.5°$N) is shown. The bottom three panels explicitly demonstrate that the equatorially trapped $n = 0, 1, 2$ modes of the ζ field are indeed excited in this case.

By moving the latitude of the sink, θ_0, from the equator to 40°N, we were able to change the relative strength of the response in the different meridional modes. This is expected since the forcing projects differently onto the different modes as one varies θ_0. On the equator, for example, $\theta_0 = 0°$ and the vortex stretching induced by the forcing is exactly asymmetric about the equator due to the Coriolis parameter asymmetry about the equator. The forcing is therefore orthogonal to, and has zero projection onto, the $n = 0$ mixed Rossby–gravity wave (MRG) mode of the system, whose vorticity structure is symmetric about the equator. For off-equatorial forcings, we do stimulate the $n = 0$ mode, though the $n = 1, 2$ modes were excited more strongly for all values of θ_0 that we tried: presumably this is due to the particular choice of forcing structure and phase speed that we use. Forcings with $\theta_0 > 40°$, well outside the equatorial waveguide, excite a weak equatorial response.

b. *Application to observed tropical cyclone wakes*

The resemblance of the disturbances in our numerical experiments to those seen in the observations leads us to hypothesize that in observed cases of Rossby wave radiation from TCs in the western North Pacific, result-

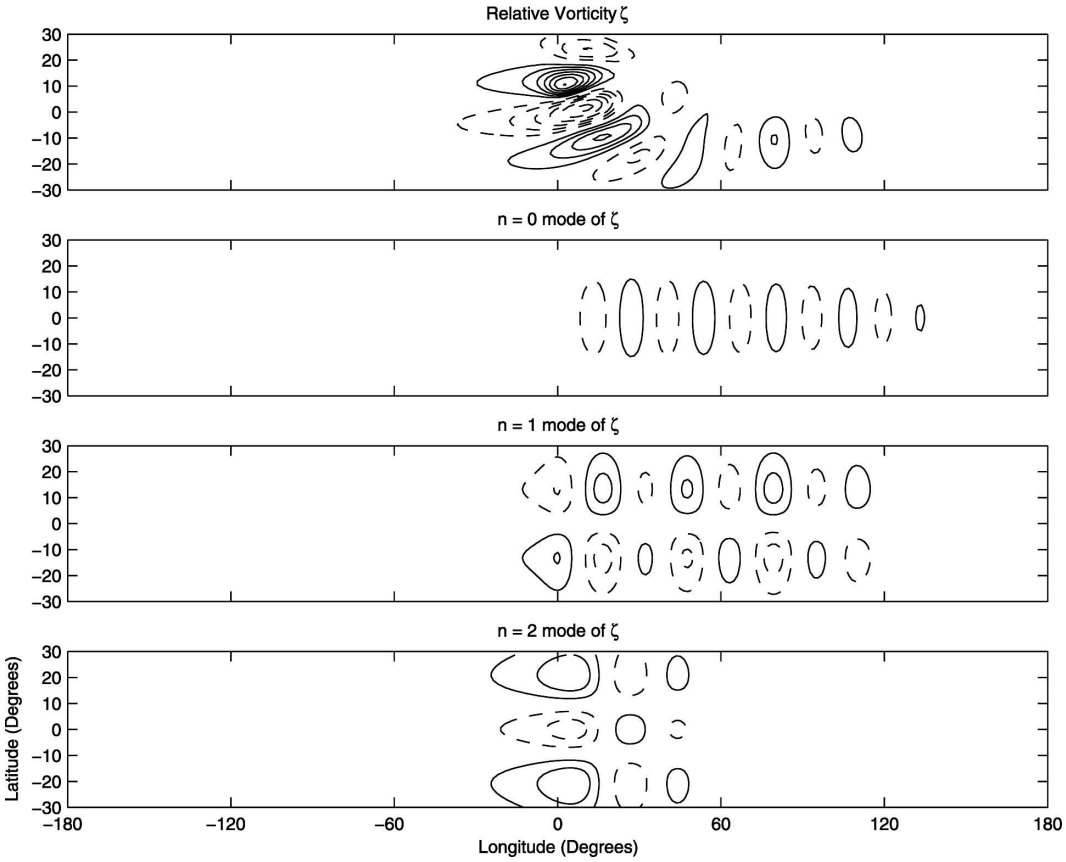

FIG. 6. Results from a typical linear run (Ro = 0.56) with a low-latitude forcing ($\theta_0 = 7.5°$N) and $U = +5$ m s^{-1} after reaching steady state. (top) The full relative vorticity field ζ, with a contour interval of 2.0×10^{-6} s^{-1}. The first three equatorially trapped Rossby wave modes: (upper middle) the $n = 0$ MRG, (lower middle) $n = 1$, and (bottom) $n = 2$ decompositions of the full ζ field. The contour interval for these panels is 1.0×10^{-6} s^{-1}.

ing in the generation of TD-type disturbances and in some cases genesis of a second TC, the wavelength of the disturbance is set by the dynamics of the steady solution. The essential features of the steady solution take only a couple of days to be established in our experiments. This is short compared to the lifetimes of the disturbances in question, making this hypothesis at least plausible. The actual disturbances need not be completely steady (as they are not in nature) for this hypothesis to be correct.

Using Eq. (8), values of U in the range of 2–4 m s^{-1} give wavelengths of 2000–3000 km, consistent with observed wavelengths of TD-type disturbances and multiple cyclone events. Some care is needed in interpreting this number in the context of observations of the real atmosphere. While it might at first appear straightforward to interpret $-U$ as the propagation speed of a tropical cyclone necessary for a wave of a given wavelength to be radiated, this would be incorrect. The environmental flow velocity U that determines the wavelength is the difference between the zonal velocity of the steering flow of the radiated Rossby waves and that of the TC.

The tracks of tropical cyclones are influenced by several factors, but the dominant influence in most cases is advection by a steering flow, which is reasonably well captured by the vertical mean environmental flow over a deep layer (e.g., Chan 2005, and references therein). For the sake of argument, consider a case in which the environmental flow is uniform with height and the TC is passively advected at precisely that velocity. In that case, the environmental flow *relative to the TC* would be zero. Here $U = 0$ would be the appropriate velocity to use in Eq. (6), so in that case we would not expect to observe a steady solution.

One plausible way to extend the linear arguments presented above to the observed cases might be to consider that the velocity of the steering flow relevant to the radiated Rossby waves might, in fact, be different from the translation velocity of the TC. We recognize that it may not be easy, in practice, to quantify this difference since it is difficult to compute the effective

steering level for a realistic TD-type disturbance on a realistic basic flow. Nonetheless, we can think of at least two reasons that the two steering flows might differ. One is the self-induced "beta drift" component of the TC translation velocity, which can have a magnitude on the order of 2 m s^{-1} (Chan 2005). On the other hand, the dynamics that induce this drift are precisely the same dynamics that induce the Rossby wave radiation that generates the second cyclonic disturbance, so it is not entirely obvious why this (already somewhat small) velocity component would not contribute to the steering of the second disturbance. The other possibility is that the radiated waves are steered by a flow that samples the environmental wind structure in a different way than does the TC. This could occur in the presence of either horizontal or vertical shear.

There is considerable evidence in the observational literature that western Pacific TD-type disturbances have most of their amplitude at low levels (e.g., Reed and Recker 1971; Lau and Lau 1990). Sobel and Bretherton (1999), in particular, showed that the propagation of the disturbances could on average be well captured by considering only layerwise barotropic dynamics at 850 hPa. If the TCs are steered by a deeper layer mean flow than the waves are, and the disturbances occur in an environment of easterly shear, the TC will feel a steering flow westward relative to that of the waves, corresponding to the case $U > 0$ in our simulations. Much of the region in the western North Pacific where TD-type disturbances and multiple cyclone events typically occur is characterized by easterly shear, with persistent low-level westerlies and upper-level easterlies (e.g., Holland 1995; Ritchie and Holland 1999).

Horizontal shear might also lead to the necessary difference between the steering flows. Often, TCs develop in a monsoon trough environment characterized by large-scale cyclonic vorticity at low levels, which is often manifested by westerlies to the south and easterlies to the north. In the linear regime, the wave train develops to the southeast of the TC (the nonlinear regime is somewhat different in this respect, as shown below). This places the secondary vorticity maximum in an environment of low-level flow, which is westerly with respect to that of the TC, the sign which corresponds to $U > 0$ in our simulations.

The arguments above lead to some predictions that can, at least in principle, be tested by analysis of observational data. If the vertical shear explanation is the correct one, the stationary-state TC wave radiation mechanism will only occur when the vertical shear of the environmental wind is easterly, and the wavelength of the resulting waves will be larger for larger shear. The dependence of the wavelength on shear, however, is not expected to be strong, as $\lambda_{\text{stationary}}$ is a relatively weak function of U [cf. Eq. (8)]. If the horizontal shear explanation is correct, then multiple cyclone events will occur primarily in regions of large-scale cyclonic vorticity at low levels (something already known to be generally true) whatever the sign of the vertical shear. Of course, combinations of the two mechanisms are possible.

However, independent of whether the vertical or the horizontal shear plays a greater role, our theory predicts that the wavelength is independent of the size of the TC. This appears to be true in our experiments—notice the tight clustering of the T42 and T85 results. On the other hand, the amplitude of the radiated waves is expected to be an increasing function of the TC size and intensity, by standard arguments (Rhines 1975).

c. *Nonlinear regime, Ro > 1*

While one would not expect linear arguments to be valid as the vortex amplitude is increased and the wave train in the wake of the cyclone becomes more nonlinear, we have found that most of the key features of the linear solutions survive in the nonlinear regime. This is illustrated in Fig. 7, for which the average Rossby number for the three cases is 2.16; this figure can be directly contrasted with Fig. 1, its linear counterpart. A wave train forms for $U > 0$ and does not for $U \leq 0$. Occasionally during the nonlinear runs, vortex shedding occurs (e.g., see Hsu and Plumb 2000) and the ζ field does not reach a true steady state as it does in the linear case. The zonal projections of Eq. (10) for the modes we looked at ($n = 0, 1, 2$) do, however, reach approximately steady states. We use these to determine the peak-to-peak distances included in Fig. 8. The peak-to-peak distance is found using the same technique as described in section 3.

As the forcing is strengthened and the dynamics become more nonlinear, the wave trains generally exhibit a more zonal structure with less northwest–southeast tilt. This is thought to be due to enhanced advection of the secondary vortices by the enhanced westerly flow equatorward of the primary cyclonic vortex. This broadly improves the agreement with observations; in the linear cases, the secondary cyclonic disturbance was located in the Southern Hemisphere for a mass sink at 15°N, whereas observed TD-type disturbances and multiple cyclone events are generally restricted to one hemisphere. The wave train also becomes more zonal as U is increased. As in the linear cases, in these nonlinear runs the results are qualitatively independent of

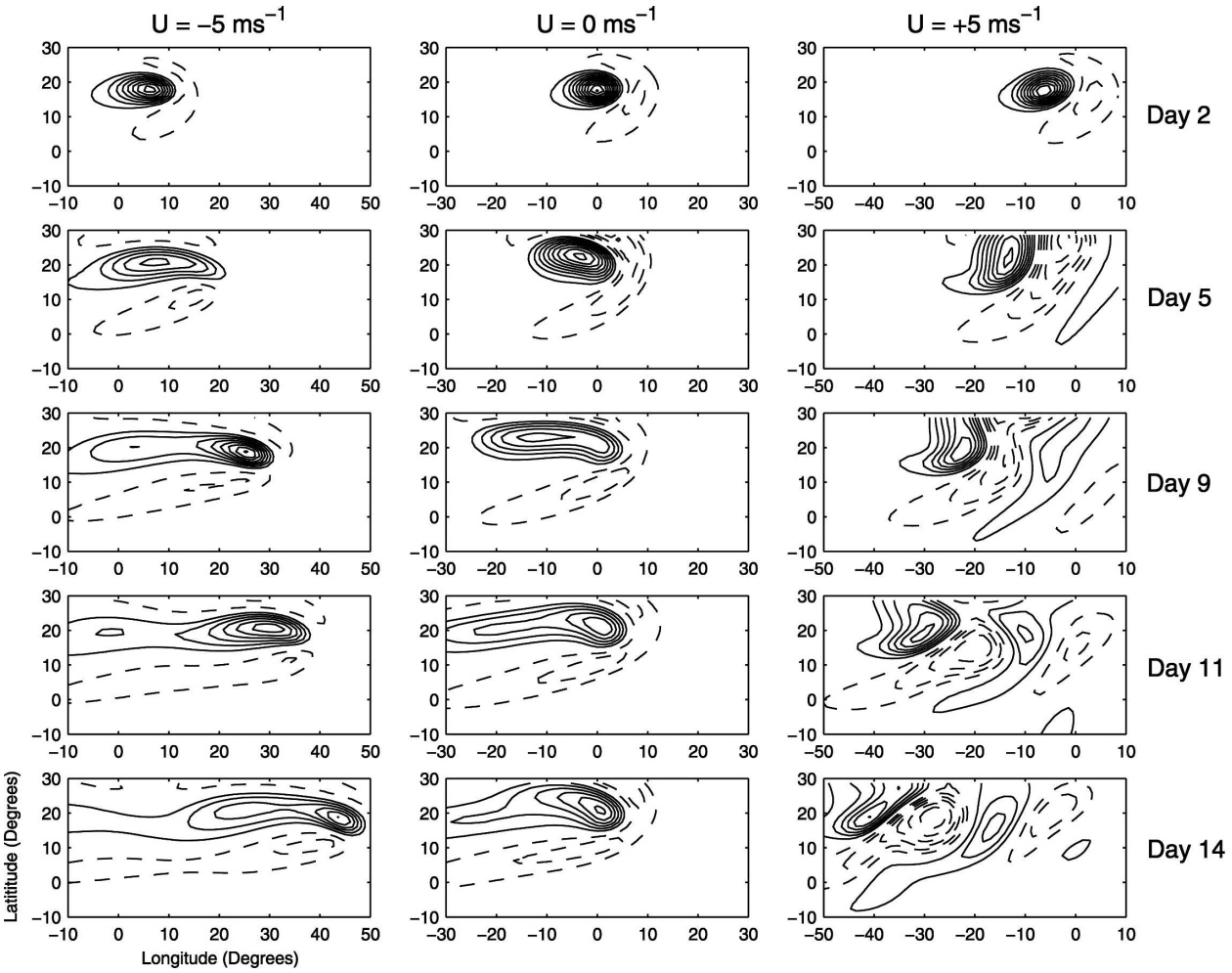

FIG. 7. As in Fig. 1 but for nonlinear experiments with larger forcing amplitude, resulting in an average Rossby number Ro = 2.16. Contour interval here is 1×10^{-5} s^{-1}.

the forcing latitude θ_0, and equatorially trapped modes are excited as well (not shown). As expected, the strength of these modes' signal increases with magnitude of the forcing.

For sufficiently small values of the hyperdiffusion coefficient and $U < 0$, there is a regime in which the forced vortex periodically separates from the forcing and moves away to the northwest where it disperses and dissipates as a new vortex is generated at the forcing location, resulting in a periodic or quasiperiodic cycle. Similar behavior is documented, for a stationary forcing, in Zhou and Sobel (2006). This behavior is likely to be of little relevance to the observed phenomena of TD-type disturbances and multiple cyclone events, as in observations the secondary vortices appear to the east or southeast of the TC. The values of the hyperdiffusion coefficient used in the figures shown here were chosen as small as possible so as retain the nonlinear dynamics in the model, while damping out this behavior.

Figure 8 shows the separation distances predicted by Eq. (8) versus the peak-to-peak wavelength for various values of U, n, and resolution. The average value of Ro for the data presented is 2.16.

As might be expected, the agreement in Fig. 8 is not as close as in the linear cases. Nonetheless, it is close enough to suggest that the spatial scale of the disturbances is still, in this moderately nonlinear regime, set by the dynamics of the linear stationary solutions. Nonlinear dynamics modify the structure of the flow somewhat, particularly the degree of zonality versus northwest–southeast tilt, and to a lesser degree the wavelength. The results of the T85 and T42 simulations remain fairly tightly clustered, suggesting that the separation distance remains essentially independent of the size of the initial TC.

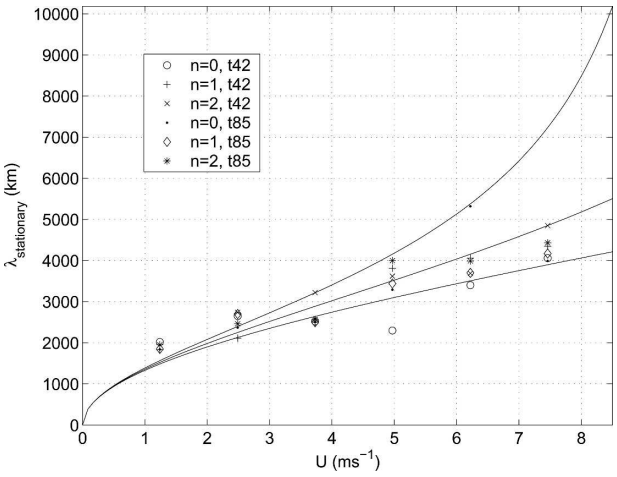

FIG. 8. As in Fig. 5 but for the nonlinear experiments in Fig. 7 at larger forcing amplitude.

4. Conclusions

We have proposed a theory for the zonal separation distance during a multiple cyclone event. The idea was demonstrated using shallow-water numerical experiments on a sphere, forced by an imposed mass sink translated zonally. Eastward Rossby wave energy dispersion from a vortex whose steering flow is westward with respect to that of the short wavelength Rossby waves results in a wave train to the east or southeast of the initial vortex. The scale is selected by the dynamics of the steady solution in the frame moving with the vortex. In our experiments, the relevant flow velocity in the expression for the stationary wavelength, Eq. (8), is minus that at which the mass sink is moved. Coherent wave trains are obtained for westward-moving mass sinks, but not stationary or eastward-moving ones, in agreement with the stationary solution predicted by linear theory. The wavelengths obtained also agree quantitatively with the stationary linear solutions.

These results suggest that the wavelength of observed TD-type disturbances and multiple cyclone events are set by the dynamics of the steady solution, with the relevant velocity being the difference between the steering flow felt by the waves and that felt by the TC. These steering flows can be different in the presence of vertical shear if the TC is steered by a deeper vertical mean flow than the waves are, or in the presence of low-level cyclonic horizontal shear even if their steering levels are the same. There is evidence that both conditions may be met, for example, in the western North Pacific, with the shears having the correct sign (easterly vertical shear or cyclonic horizontal shear) to generate wave trains according to our argument. It is difficult to calculate the relevant steering flows in a precise way, but given the substantial vertical and horizontal shears in the western North Pacific monsoon region, it does not seem unreasonable to expect that the relevant difference might reach values of 2–4 $\mathrm{m\,s^{-1}}$, which is the magnitude necessary to generate waves of the observed 2000–3000-km wavelength. The dependence of the wavelength on this difference is relatively weak, so it is not necessary to estimate it very precisely.

Our results suggest that nonlinearity can alter the structure of the wave trains, making them more zonally oriented, as opposed to northwest–southeast oriented. The essential scale selection mechanism is not altered by moderate nonlinearity.

The argument presented here leads to several predictions, which are in principle testable using observational data. One is that the wavelength of the disturbances is independent of the size of the primary TC, although the amplitude is not. Another is that the stationary-state TC wave radiation mechanism should occur either in regions of easterly shear or cyclonic low-level horizontal shear. A third is that the wavelength of the disturbances should increase weakly with the magnitude of the shear. Work is currently underway to evaluate these predictions using existing datasets.

Acknowledgments. This work was supported by NASA Grants NNG04G032A and NNX07AP74A. KDK acknowledges support from the U.S. National Science Foundation, through a fellowship in the IGERT Joint Program in Applied Mathematics and Earth and Environmental Science at Columbia University.

REFERENCES

Aiyyer, A., and J. Molinari, 2003: Evolution of mixed Rossby–gravity waves in idealized MJO environments. *J. Atmos. Sci.,* **60,** 2837–2855.

Briegel, L. M., and W. M. Frank, 1997: Large-scale influences on tropical cyclogenesis in the western North Pacific. *Mon. Wea. Rev.,* **125,** 1397–1413.

Carr, L., and R. Elsberry, 1995: Monsoonal interactions leading to sudden tropical cyclone track changes. *Mon. Wea. Rev.,* **123,** 265–289.

Chan, J., 2005: The physics of tropical cyclone motion. *Annu. Rev. Fluid Mech.,* **37,** 99–128.

Chang, C.-P., J.-M. Chen, P. Harr, and L. Carr, 1996: Northwestward-propagating wave patterns over the tropical western North Pacific during summer. *Mon. Wea. Rev.,* **124,** 2245–2266.

Chang, H.-R., and P. Webster, 1990: Energy accumulation and emanation at low latitudes. Part II: Nonlinear response to strong episodic equatorial forcing. *J. Atmos. Sci.,* **47,** 2624–2644.

——, and P. J. Webster, 1995: Energy accumulation and emanation at low latitudes. Part III: Forward and backward accumulation. *J. Atmos. Sci.,* **52,** 2384–2403.

Davidson, N., and H. Hendon, 1989: Downstream development

in the Southern Hemisphere monsoon during FGGE/WMONEX. *Mon. Wea. Rev.,* **117,** 1458–1470.

Dickinson, M., and J. Molinari, 2002: Mixed Rossby–gravity waves and western Pacific tropical cyclogenesis. Part I: Synoptic evolution. *J. Atmos. Sci.,* **59,** 2183–2196.

Dunkerton, T., and M. Baldwin, 1995: Observation of 3–6-day meridional wind oscillations over the tropical Pacific, 1973–1992: Horizontal structure and propagation. *J. Atmos. Sci.,* **52,** 1585–1601.

Ferriera, R. N., and W. Schubert, 1997: Barotropic aspects of ITCZ breakdown. *J. Atmos. Sci.,* **54,** 261–285.

Flierl, G., M. Stern, and J. Whitehead, 1983: The physical significance of modons: Laboratory experiments and general integral constraints. *Dyn. Atmos. Oceans,* **7,** 233–263.

Frank, W., 1982: Large-scale characteristics of tropical cyclones. *Mon. Wea. Rev.,* **110,** 572–586.

Gill, A., 1982: *Atmosphere–Ocean Dynamics.* Academic Press, 662 pp.

Hack, J. J., and R. Jakob, 1992: Description of a global shallow water model based on spectral transform method. NCAR Tech. Note NCAR/TN-343+STR, 41 pp.

Holland, G., 1995: Scale interaction in the western Pacific monsoon. *Meteor. Atmos. Phys.,* **56,** 57–79.

Hsu, C., and R. Plumb, 2000: Nonaxisymmetric thermally driven circulations and upper-tropospheric monsoon dynamics. *J. Atmos. Sci.,* **57,** 1255–1276.

Kuo, H.-C., J.-H. Chen, R. Williams, and C.-P. Chang, 2001: Rossby waves in zonally opposing mean flow: Behavior in northwest Pacific summer monsoon. *J. Atmos. Sci.,* **58,** 1035–1050.

Lau, K.-H., and N.-C. Lau, 1990: Observed structure and propagation characteristics of tropical summertime synoptic scale disturbances. *Mon. Wea. Rev.,* **118,** 1888–1913.

Li, T., and B. Fu, 2006: Tropical cyclogenesis associated with Rossby wave energy dispersion of a preexisting typhoon. Part I: Satellite data analyses. *J. Atmos. Sci.,* **63,** 1377–1389.

——, ——, X. Ge, B. Wang, and M. Ping, 2003: Satellite data analysis and numerical simulation of tropical cyclone formation. *Geophys. Res. Lett.,* **30,** 2122–2126.

Mapes, B., and R. Houze, 1995: Diabatic divergence profiles in western Pacific mesoscale convective systems. *J. Atmos. Sci.,* **52,** 1807–1828.

Matsuno, T., 1966: Quasi-geostrophic motions in the equatorial area. *J. Meteor. Soc. Japan,* **44,** 25–43.

McWilliams, J., and G. Flierl, 1979: On the evolution of isolated, nonlinear vortices. *J. Phys. Oceanogr.,* **9,** 1155–1182.

——, P. Gent, and N. Norton, 1986: The evolution of balanced, low-mode vortices on the β-plane. *J. Phys. Oceanogr.,* **16,** 838–855.

Nitta, T., and Y. Takayabu, 1985: Global analysis of the lower tropospheric disturbances in the Tropics during the northern summer of the FGGE year. Part II: Regional characteristics of the disturbances. *Pure Appl. Geophys.,* **123,** 272–292.

Reed, R., and E. Recker, 1971: Structure and properties of synoptic-scale wave disturbances in the equatorial western Pacific. *J. Atmos. Sci.,* **28,** 1117–1133.

Rhines, P., 1975: Waves and turbulence on a beta-plane. *J. Fluid Mech.,* **69,** 417–443.

Ritchie, E., and G. Holland, 1999: Large-scale patterns associated with tropical cyclogenesis in the western Pacific. *Mon. Wea. Rev.,* **127,** 2027–2043.

Shapiro, L. J., and K. V. Ooyama, 1990: Barotropic vortex evolution on a beta plane. *J. Atmos. Sci.,* **47,** 170–187.

Sobel, A. H., and C. Bretherton, 1999: Development of synoptic-scale disturbances over the summertime tropical northwest Pacific. *J. Atmos. Sci.,* **56,** 3106–3126.

——, and E. D. Maloney, 2000: Effect of ENSO and the MJO on western North Pacific tropical cyclones. *Geophys. Res. Lett.,* **27,** 1739–1742.

Takayabu, Y., and T. Nitta, 1993: 3–5 day period disturbances coupled with convection over the tropical Pacific Ocean. *J. Meteor. Soc. Japan,* **71,** 221–246.

Webster, P., and H.-R. Chang, 1988: Equatorial energy accumulation and emanation regions: Impacts of a zonally varying basic state. *J. Atmos. Sci.,* **45,** 803–829.

Wheeler, M., and G. Kiladis, 1999: Convectively coupled equatorial waves: Analysis of clouds and temperature in the wavenumber–frequency domain. *J. Atmos. Sci.,* **56,** 374–399.

Zhou, B., and A. H. Sobel, 2006: Nonlinear shallow-water solutions using the weak temperature gradient approximation. *Theor. Comput. Fluid Dyn.,* **20,** 469–484.